PAPER

Characterization of plasma in RF jet interacting with water: Thomson scattering versus spectral line broadening

To cite this article: Shurik Yatom *et al* 2022 *Plasma Sources Sci. Technol.* **31** 035018

View the article online for updates and enhancements.

Plasma Sources Sci. Technol. **31** (2022) 035018 (12pp) https://doi.org/10.1088/1361-6595/ac56ed

Characterization of plasma in RF jet interacting with water: Thomson scattering versus spectral line broadening

Shurik Yatom[1,*], **Trey Oldham**[2] **and Elijah Thimsen**[2]

[1] Princeton Plasma Physics Laboratory, Princeton University, NJ, United States of America
[2] Washington University in Saint Louis, Department of Energy, Environmental & Chemical Engineering, St. Louis, MO, United States of America

E-mail: syatom@pppl.gov

Received 13 December 2021, revised 7 February 2022
Accepted for publication 21 February 2022
Published 25 March 2022

Abstract
In this work we carry out a detailed characterization of an Ar radiofrequency plasma jet interacting with liquid. The focus of the paper is measurement of the electron density by examining the Stark broadening of hydrogen Balmer α line and Thomson scattering (TS). Supporting diagnostics are done to investigate the channel evolution and movement, and gas temperature. The comparison of the two approaches shows the caveats and the advantages that should gain attention in future applications. In particular, the plasma channel dynamics have a significant impact on the TS signal and may result in physical phenomena being missed due to channel dislocations. The conclusions of the work elucidate the pitfalls for interpreting the results of TS when the discharge is a dynamic filamentary plasma. This work establishes the temporal evolution of the plasma and the gas parameters in a plasma–liquid system employed for investigation of plasma-induced electrodeless electrochemistry.

Keywords: plasma diagnostics, line broadening, Thomson scattering, plasma–liquid interaction, plasma electrochemistry

(Some figures may appear in colour only in the online journal)

1. Introduction

The diagnostics of low-temperature plasmas at high pressures often relies on optical methods. Optical emission spectroscopy (OES) is by far one of the most popular approaches. Most frequently plasma electron density (N_e) is characterized by Stark broadening of selected spectral lines, particularly the first two of the hydrogen Balmer series, i.e. H_α and H_β. To correlate the measured Stark widths to the electron density values one usually refers to tabulations, such as the work of Gigosos *et al* [1] The full-width-at-half-maximum (FWHM) and full-width-at-half-area (FWHA) in the above work are given for H_α, H_β and H_γ lines as a function of electron density. In principle, the line emission can also be used to measure the electron temperature (T_e) by way of the Boltzmann plot approach [2]. However, for low-temperature plasma the measured value is actually the excitation temperature (T_{exc}), which approaches T_e when the condition for local thermodynamic equilibrium (LTE) or a partial LTE is realized [3]. This condition is usually fulfilled for sufficiently high N_e [4], which is not true for most of atmospheric pressure plasma jets (APPJs) that have $N_e < 10^{23}$ m^{-3}. Consequently, in many atmospheric non-equilibrium plasmas the electron temperature cannot be measured by spectral line emission.

Another technique that emerges as popular in low-temperature plasma community is Thomson scattering (TS). TS is advantageous because it constitutes a direct measurement of N_e and T_e and is routinely used to study low-temperature plasma sources [5, 6]. TS was applied for plasma characterization in free-space plasma jet [7] and plasma-interaction with liquid [8] as well as dielectric and conducting targets [9].

* Author to whom any correspondence should be addressed.

The body of work that contains direct comparisons of the two above approaches, i.e. line broadening vs TS is somewhat limited. Palomares *et al* [10] have conducted a comparative study between H_β broadening and TS for plasma at low-to-intermediate pressure (1.5–30 Torr) and plasma electron densities of $6.8 \times 10^{18} \leqslant N_e \leqslant 2.5 \times 10^{19}$ m^{-3}, which included detailed analysis of line broadening mechanisms. The conclusion highlighted the importance of knowing the gas temperature for correct line broadening analysis and showed an agreement between N_e as determined by TS and H_β Stark width within 20% error margin. A recent study [11] investigated the impact of grounding in atmospheric pressure plasma–liquid system by means of TS and used H_β line broadening to verify the TS results, however an in-depth comparison of the two approaches was out of scope of the work. In that work the authors used a pulsed 5 μs Ar jet operated at 16 kHz frequency in contact with water. The water was grounded through a series of resistors with values between 1–680 kOhm, to mimic different liquid conductivities. It was found that overall plasma density and temperature decrease with increasing resistance. The density and temperature values were found to be in range 10^{20}–10^{21} m^{-3} and 1–3.5 eV respectively. In a similar study [12] same team of authors investigated the plasma generated by Ar jet operated by AC 5 kV generator at 23 kHz. The maximum electron densities and temperatures of 6.0–6.3 $\times$ 10^{20} m^{-3} and 3.1–3.3 eV for the floating liquid case and 1.1×10^{21} m^{-3} and 4.3 eV in the grounded liquid case. A plasma He jet impinging on water was also characterized in the recent work [9]. This jet was powered by a square 6 kV pulse, with duration of 1 μs and supplied at frequency of 5 kHz. The maximum plasma density and temperature determined to be $\sim 1.7 \times 10^{23}$ m^{-3} and $\sim$3 eV, respectively. A nanosecond pin-to-liquid discharge in He was studied with TS in the work by Simeni *et al* [8], at the pressure of 100 Torr. Maximum plasma densities and temperatures measured were $\sim 10^{21}$ m^{-3} and 3.5 eV. We are not aware of works where an radiofrequency (RF) jet impinging on water was investigated.

In this work we investigate an atmospheric pressure plasma–liquid system, where a RF Ar plasma jet impinges on a floating liquid. We conduct a detailed study of the discharge evolution by way of fast intensified imaging, measurement of the gas temperature, and plasma characterization. The measured gas temperature is used for precise estimation of line broadening mechanisms and fast imaging allows for the consideration of the impact that plasma channel oscillations have on the measurements. An analysis of line broadening is done to compare the measured density to the one obtained via TS method. In this work we examine the H_α line rather than H_β. Generally, H_β is widely analyzed, owing to the more straight-forward tabulation and lower threshold for broadening detection. However, in some situations the use of H_β is either challenging or not possible. For instance, in the case of this work the H_β emission had a very low signal-to-noise ratio (SNR) which prevented data fitting and any meaningful interpretation of the line shape analysis. Also, in conditions where the electron density was sufficiently high the H_β profile was too broad, making the line-shape fitting problematic [4, 13]. It is therefore important to study and compare H_α broadening as well. The caveats of the two approaches (TS vs H_α Stark broadening) are discussed and the outcomes are compared throughout a cycle of the plasma jet ignition and evolution.

The aim of this work is the detailed study of the plasma parameters in the given plasma–liquid system, which was developed by the co-authors in Washington University in Saint Louis, to study plasma-induced liquid electrochemistry. More specifically, the goal was to identify the relationship between the state variables of the plasma (e.g. T_e and N_e) and the reduction potential measured in solution, which is the key parameter that determines the rate and direction of electrochemical reactions. While similar APPJs have been demonstrated to promote reduction–oxidation reactions, a correlation between the plasma parameters and the reduction potential has not been clearly established, hindering the ability to achieve controlled chemical transformations using plasma–liquid systems. This is due to, in part, the challenges of performing diagnostics on low-temperature plasmas operating at atmospheric pressure. Low temperature plasma jets in contact with liquids are not generally known to promote selective redox reactions involving organic molecules, thus our previous result of the selective reduction of an organic compound [14] is of interest for organic chemistry promoted by plasma–liquid interfaces. Full characterization of the low temperature plasma that is capable of selective organic reactions is critical to establish the plasma parameters that provide this desirable result for the sake of reproduction by plasmas generated by other sources. Furthermore, those parameters can provide a reference point for what is required on the plasma side of the interface to promote electrodeless organic reductions in solution.

2. Experimental

2.1. RF jet and the liquid setup

The plasma source in the experiment was an APPJ, powered by a 13.56 MHz RF power supply, (T & C Power Conversion, AG 0613) connected to an impedance matching network (T & C Power Conversion, AIT-600 RF Auto Tuner). The power supply was operated with 20% duty cycle, with pulse active time of 10 μs, followed by 40 μs 'off-time'. The duty cycle was controlled by a digital delay pulse generator (BNC 575), which also served for synchronization of laser diagnostics and the detector. The powered electrode is a tungsten rod with a sharp conical edge. The powered electrode is contained inside a fused silica tube. The ground electrode is an aluminum ring, mounted on the outside of the tube. The jet is sustained in the Ar gas, flowing through the tube at a flow rate of 1 standard liter per minute. In experiments the jet was suspended above the dish filled with the treated liquid, on a 3D translational stage. The dish was connected to a large reservoir with the liquid, which was filled and positioned to allow the liquid to slightly overflow from the sides of the dish. The liquid overflow ensured that the level of the liquid in the dish maintained a constant level during the experiments. The sketch of the experimental setup is shown at figure 1.

The liquid solution was selected to reproduce our previous result of the selective reduction of an organic compound by plasma–liquid interface. [14] An aqueous 75 μM indigo

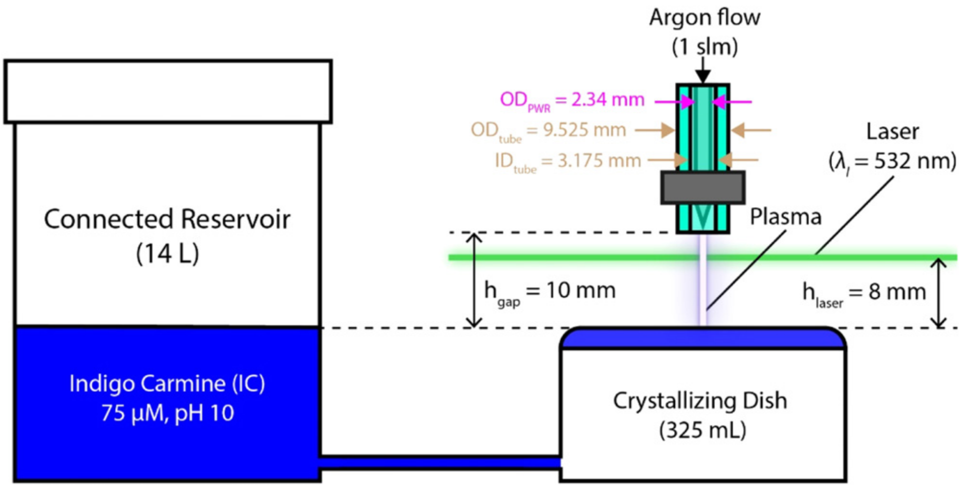

Figure 1. Schematic arrangement for RF jet and liquid in dish setup.

carmine (IC) solution with an adjusted pH of 10 was used to fill a reservoir and crystallizing dish with nominal solution volumes of 14 l and 325 ml, respectively. The measured pH of the untreated IC solution was 10.1, which decreased to 9.9 following the laser alignment procedure and Thomson data acquisition. The measured conductivity of the untreated IC solution was 75.5 μS cm^{-1}, which increased to 205 μS cm^{-1} after the laser alignment procedure and collecting the Thomson data (approximately 25–30 min).

It is possible that the change in liquids conductivity may incur variation in plasma parameters. The given setup was not fit for a constant swapping of water in the dish in a way that would maintain the liquid level constant in order not to promote movement of the plasma channel, as well as keeping the conductivity and pH constant too. The second-best strategy is to change the solution after each measurement, so that the change in conductivity would be the same for every datapoint acquired. The solution contained in the dish was replaced with a fresh one after each measurement (single cycle of laser + emission alignment and Thomson signal collection) .

2.2. Thomson scattering

Laser TS is commonly employed to measure the electron density and electron energy distribution function. The TS signal is elastic scattering of laser beam on free electrons which is broadened due to the electron's velocity. To facilitate TS diagnostics we use the setup inspired by the work of Klarenaar *et al* [15], as described below and pictured at figure 2. The laser (Continuum SL-III, operating at 532 nm, pulse length 8 ns, repetition rate 10 Hz) is focused on the region of interest, with a $f = 1$ m lens. After passing through the plasma the beam was terminated in a beam dump. The region of interest is imaged with a $f = 0.15$ m lens, on a pinhole (200 μm), acting as a spatial filter. Irises are used to decrease the amount of stray light from the reactor. A volume Bragg notch filter (BNF) is used to reject the strong Rayleigh component from the scattered light. The Rayleigh scattering is the elastic scattering of the laser photons on the neutrals, which typically have a very high density in atmospheric plasmas, due to their low degree of ionization. Since the neutral temperature in atmospheric plasma jets is usually very low—the width of the Rayleigh component is quite narrow and can be filtered out by using a triple-grating spectrometer or a specialized filter. In our setup a reflecting volume Bragg grating (VBG) is specified to block light with an optical density of 4 with a FWHM of 5–8 cm^{-1} (≡0.14–0.23 nm). The transmission of the filter outside the blocking region is 80%. The reflected wavelength can be tuned by rotating the filter. Setting an angle of 6° between the filter normal and the direction of the incoming light results in the reflection of 532 nm light, which is the operating wavelength of the laser. The main drawback of the VBG filter is the small angular acceptance of less than 0.1°, therefore, adequate collimation of the scattered light is necessary. This is achieved by placing another lens, forming a telescope configuration. The collimated light then passes through the VBG and subsequently focused on the entrance slit of a monochromator (Spectra Pro HRS750), coupled with an iCCD camera (PIMax 3) as a 2D detector (1024 × 1024 pixels). The monochromator grating is a ruled 1200 G mm^{-1} grating, the slit was set at 100 μm, the corresponding instrumental width is 1.12 Å and the dispersion relation 0.124 Å/px at (532 nm).

The collection of the Thomson signal required an accumulation of 10 000 laser shots, i.e. 17 min acquisition period of the scattered Thomson signal on the iCCD chip. A plasma channel in contact with the liquid surface is a very dynamic system and the position of the channel is prone to variation. Before every measurement an alignment procedure was conducted. The aims of the procedure are (1) to ensure optimal overlap of the laser beam and the plasma channel and (2) ensure the alignment of the plasma channel with respect to the detection line. To find the optimal position of the plasma channel with respect to the laser beam we use Rayleigh scattering. Rayleigh scattering signal is minimal when the laser probes the hottest region of the channel. Collecting Rayleigh signal is much faster than Thomson or Raman, therefore this is the most convenient approach for alignment. It requires an assumption that the hottest part of the channel is also where the electron

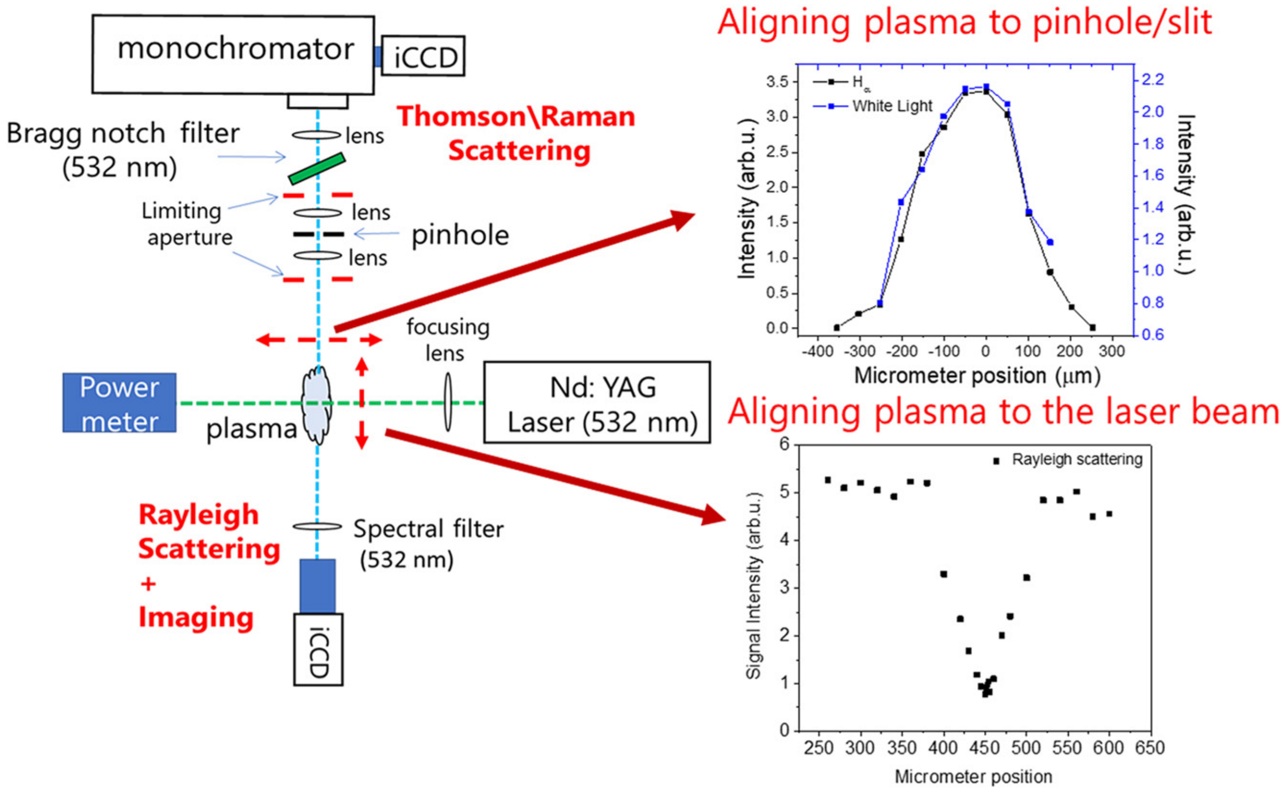

Figure 2. Schematic arrangement of the laser and detection setup. The right-side plots show the arrangement procedure that was employed before each TS datapoint collection to ensure optimal alignment of the laser to the plasma and plasma to the monochromator.

density is maximal, e.g. the heating of the gas neutrals is via electron collisions, which is a reasonable assumption in our opinion. To observe Rayleigh signal the angle of the BNF is slightly changed so that the laser photons are not rejected. The plasma channel is then moved in the direction perpendicular to the laser beam in steps of 25.4 μm, using a micrometer translational stage. The acquired signals are processed 'live' to find the micrometer position that corresponds to minimal Rayleigh signal i.e. the hottest location in the plasma. In order to align the plasma channel to the monochromator slit we move the plasma channel along the laser beam, in the direction normal to the detection axis. This is also done in steps of 25.4 μm, using a micrometer translational stage. The optimal position corresponds to peak emission of white light and/or H_α line (both were found to correlate very well). The above alignment procedure was carried out swiftly, with the data processed in real time. The directions of translations are indicated on figure 2 with dotted red lines and the corresponding Rayleigh and emission signals vs micrometer position are also shown at figure 2. After the identification of optimal position on both axis—the angle of BNF was adjusted back, to ensure rejection of the central laser wavelength. At this point the alignment procedure is completed and collection of Thomson signal can commence. The whole process—alignment and Thomson added up to be approximately 25–30 min.

The laser beam waist (spot size) is determined by measuring the energy of the laser pulse behind a moving a sharp and straight blade. The blade is moved in steps of 25.4 μm to gradually block the laser beam and prevent light from reaching the power-meter. This exercise yields a curve of measured laser pulse energy vs block position. The derivative of this curve with respect to position/spatial coordinate is the spatial distribution of the laser energy, which closely resembles a Gaussian. The size of the laser spot is in this case is the full-width-at-tenth-maximum. The operating laser pulse energy was selected to be 60 mJ, which corresponds to a fluence value of $F_{\mathrm{exp}} = 7.5 \times 10^5$ J m^{-2}. The critical fluence estimated to be $F_{\mathrm{crit}} = 1.35 \times 10^6$ J m^{-2} (for of $N_e = 1 \times 10^{22}$ m^{-3} and $T_e = 1$ eV) using the formalism developed in the work of Carbone *et al* [16]. In addition, we have collected and analyzed TS signal in a single plasma condition, for different laser pulse energy, from 35 to 170 mJ to check that the selected energy does not perturb the jet plasma by artificial heating and/or photoionization. Figure 3 shows the calculated increase (ΔN_e and ΔT_e) to the measured values as a function of laser fluence. For pulse energies of 35, 50, and 70 mJ there is no increase in measured N_e and T_e, beyond experimental error, but pulse energies of 130 and 170 mJ resulted in significant heating and photoionization.

2.3. Spectral line emission

For spectral line analysis the same setup was employed, but the slit width was set at 50 μm and the 2400 G mm^{-1} grating was used, the corresponding instrumental width was measured to be 0.32 Å. The idea to use the same setup from the TS experiments, despite having unnecessary optical elements for OES, is to maintain an identical optical path for collection. The

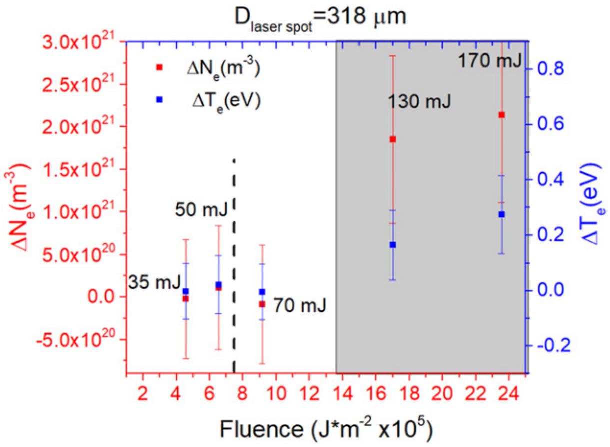

Figure 3. Measured heating and photoionization as a function of laser fluence. The black dashed vertical line indicates the fluence used in experiment, corresponding to laser pulse energy of 60 mJ. The greyed-out region indicates the fluence range that exceeds the critical value calculated for the $N_e = 1 \times 10^{22}$ m^{-3} and $T_e = 1$ eV.

calibration of the dispersion relation was done with a Hg(Ar) spectral calibration lamp. The response function of the gratings was calibrated using an integrating sphere light source (Labsphere URS-600).

2.4. Rayleigh scattering

Rayleigh scattering temperature measurements in this work were done with 532 nm wavelength pulse supplied by Continuum SLIII laser. The laser beam is observed in a direction normal to the laser beam with an iCCD camera (PIMAX 3), equipped with a 532 nm filter, to separate the elastically scattered photons from the plasma emission. It is important to note that the polarization of the laser beam should be orthogonal to the observation direction, to ensure optimal Rayleigh scattering signal. The experimental arrangement is pictured in figure 2.

2.5. Imaging

The imaging of the plasma channel is done by using the iCCD camera, equipped with an objective lens. One thousand images were obtained composed of 700 accumulations, with an exposure of 20 ns each and timestep of 20 ns as well, thus spanning a temporal segment of 20 μs to capture the plasma emission during the 'RF ON' period and the first 10 μs of the subsequent 'RF OFF' period. The purpose of imaging is to be able to track the evolution of the plasma channel and its movement. The temporal behavior of the plasma channel is then used to interpret the measurements of the plasma characteristics. This is imperative for methods that rely on intersection of the laser beam with the plasma filament, e.g. TS, particularly when the plasma is exhibiting oscillatory behavior. It is important to note that the imaging was performed in a direction perpendicular to the laser beam (see figure 2), therefore the perceived movement/oscillation of the channel position is along the path of the laser beam, not across it.

3. Analysis and results

3.1. Light emission

The evolution of the emission and the plasma channel is shown in figure 4. The onset of the emission is observed at a time delay of approximately 1.3 μs with respect to the 'RF on' pulse start (figure 4(a)), meaning that ignition of the plasma requires heating by preceding RF cycles. The emission originates at the tip of the electrode but quickly 'climbs' and hugs the needle electrode (figures 4(b)–(e)). After the ignition the plasma channel propagates towards the liquid, reaching the liquid boundary within 0.8 to 0.9 μs (figure 4(g)). At the end of the 'RF on' cycle the channel exhibits partial retraction from the liquid, i.e. the bright emission near the liquid surface diminishes and the region gradually becomes darker (figures 4(m)–(q)). Eventually, the channel becomes dislodged from the electrode and the emitted light contracts towards the center (figures 4(r)–(t)). The emission is mostly gone approximately 10 μs into the afterglow, or equivalently $\sim$10 μs after the cycle is RF switched off. The images were also analyzed to document oscillations and dislocations of the plasma channel at the 8 mm height above liquid position (HAL). To that end the area of 1 mm at HAL = 8 mm was selected and averaged along the vertical direction. The movement of the peak of the resulting curve was tracked as a function of time (*vide infra*).

3.2. Rayleigh scattering

The Rayleigh scattering approach is employed in this work to measure the gas temperature, which is necessary for interpretation of line broadening [17] and plasma-induced chemical kinetics [18]. The experimental approach is adopted from the work of van Gessel *et al* [19]. The intensity of elastically scattered photons (i.e. Rayleigh signal) is directly proportional to the density of scattering gas. In the case of an ideal gas, the density is inversely proportional to gas temperature, via the ideal gas law: $p = nk_B T_g$, where p is the given constant pressure, n is the number density of gas, and T_g is the temperature of the gas. Rayleigh signal is therefore related to the gas temperature via $I_{\mathrm{Rayleigh}} \sim n_g = \frac{p}{k_B T_g}$. To find the absolute value of T_g, a reference measurement at a known temperature T_{ref} so that $I_{\mathrm{ref}} \sim n_{\mathrm{ref}} = \frac{p}{k_B T_{\mathrm{ref}}}$ is necessary for calibration. When the composition of the gas employed in the reference measurement is identical to the gas in the experiment (or at least has a similar differential cross section for Rayleigh scattering), as are the experimental setup and pressure we can infer that $T_g = \frac{I_{\mathrm{ref}}}{I_{\mathrm{Rayleigh}}} T_{\mathrm{ref}}$. Figure 5(a) shows the reference image in flowing Ar gas without plasma, the reflection from the nozzle and the liquid surface are unobscured, for reference. Figure 5(b) shows the image obtained during the discharge (the nozzle and the liquid are obscured to allow accumulation of the signal on CCD without saturation). Analysis of the scattering signal along the laser beam yields the radial temperature profile as shown at figure 5(c) for different RF powers. Finally, figure 5(d) presents the temporal evolution of the gas temperature in the hottest region of the discharge channel. This

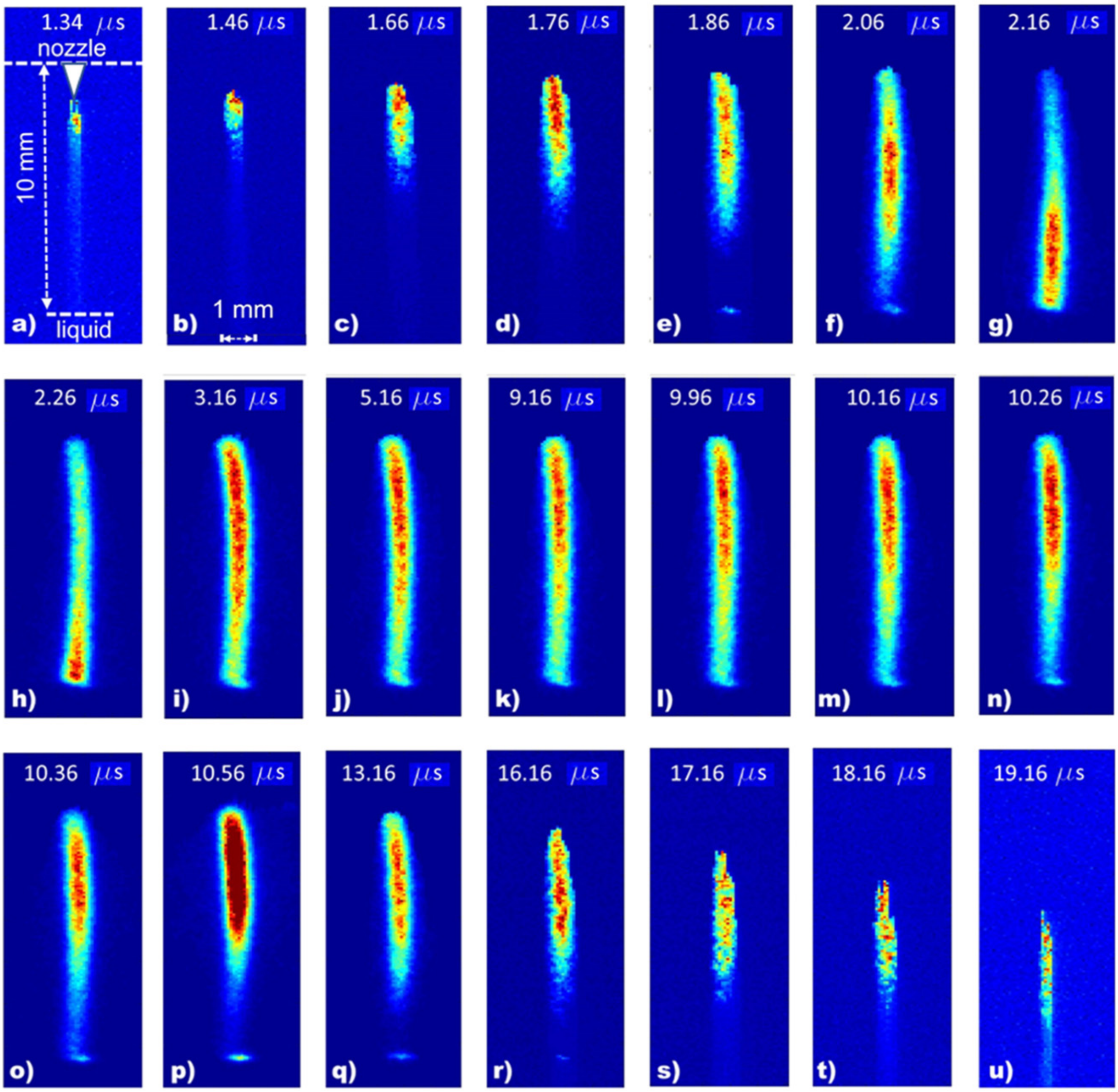

Figure 4. Imaging of the RF jet emission evolution.

temperature was used to evaluate the spectral line broadening that are directly related to gas temperature [i.e. Doppler and Van-der-Waals (VdW) widths]. No sharp changes in the peak T_g were measured during the plasma on cycle. Slight heating may be seen after the plasma channel reaches the liquid at $t = 2$ μs and after the termination of the RF pulse at $t = 10$ μs, however all measured values are within the error bars. The temperature value and the error bars were determined as the average and the standard deviation of 50 separate measurements taken for the same temporal step.

3.3. Stark width analysis

The emission spectra of the RF jet interacting with liquid featured both H_β and H_α lines. Normally, H_β is the preferred method for calculating N_e for two main reasons: (i) H_β broadening is stronger than that of H_α therefore it allows measurement of electron density at lower densities and (ii) the FWHM of H_β is less impacted by ion dynamics effects and temperature changes. However, in some cases the H_β emission is weak or obstructed by emission from other elements. In the case considered in this paper the emission of H_β was barely observable throughout most of the 10 μs 'RF on' cycle. When it was observable—the SNR was quite high, to the point that the fitting of the emission profile was compromised. Considering the above circumstances, the use of H_α line is preferable.

The analysis of H_α profile and determination of its Stark width requires an estimation of the mechanisms that cause line broadening. The VdW broadening was calculated by the

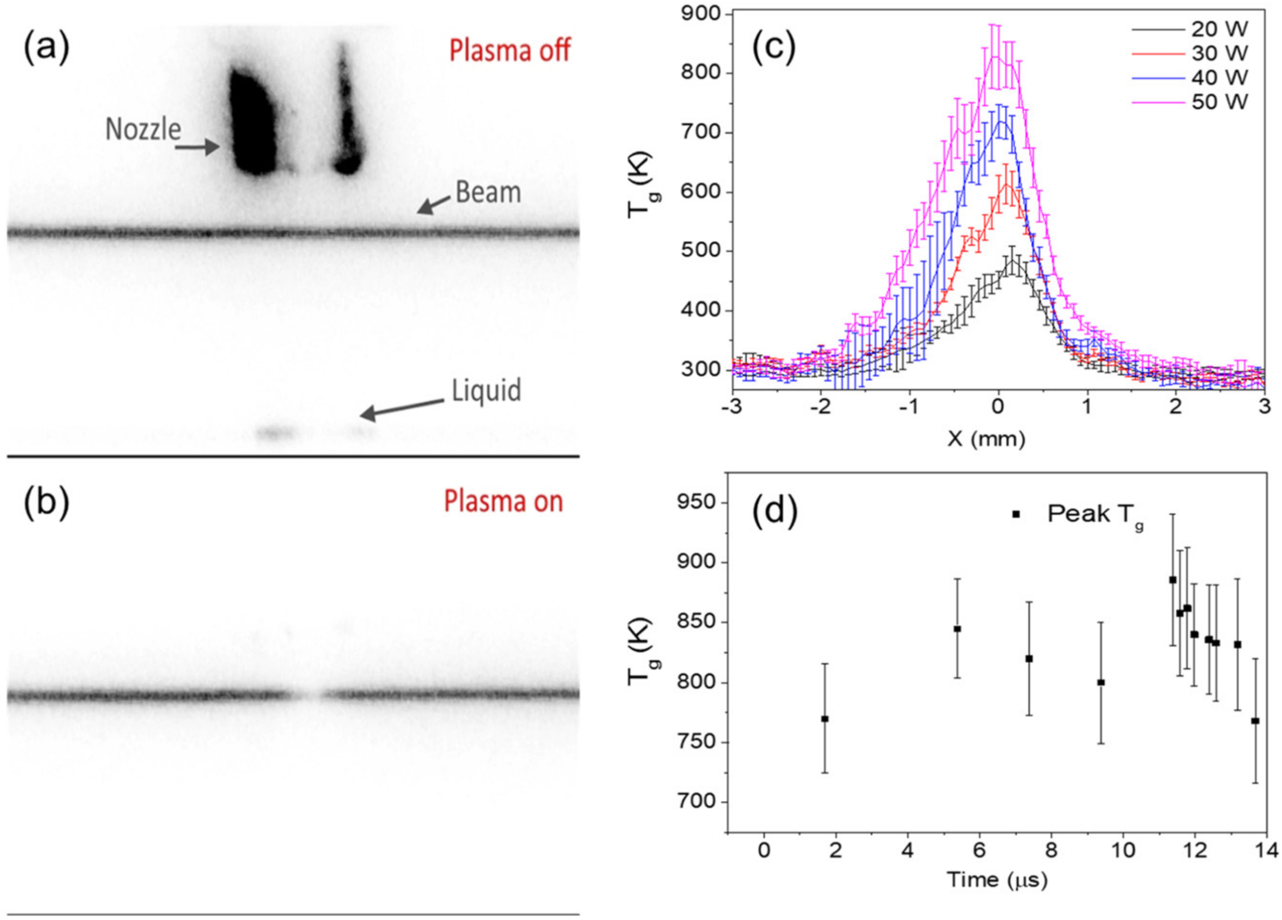

Figure 5. Gas temperature measurement with Rayleigh scattering. (a) Reference image obtained in ambient room atmosphere. (b) Rayleigh scattering image showing reduced intensity in the region of plasma–laser interaction. (c) 1D radial temperature profiles for different RF powers. (d) temporal evolution of the peak gas temperature for RF 50 W.

approach detailed in the work by Yubero *et al* [20] for atmospheric pressure plasma ($\Delta\lambda_{\mathrm{VdW}}(\mathrm{\AA}) = \frac{57.36}{T_g^{0.7}}$) and the Doppler broadening was calculated via [2] $\Delta\lambda_{\mathrm{Dopp.}}\left(\mathrm{\AA}\right) = 7.16 \times 10^{-7} \times \lambda_{\mathrm{H}_\alpha}\sqrt{\frac{T_g(K)}{m_{\mathrm{H}}(\mathrm{amu})}}$. Resonance broadening is considered negligible, in this case also because density of hydrogen is low. Table 1 shows the calculated values of broadening mechanisms used for deconvolution of Stark profiles from the experimental profiles. It is assumed that the experimental profile is a Voigt profile, where the Gaussian component is due to instrumental and Doppler contributions and the Lorentzian component is due to Stark and VdW contributions. This approach implies that Stark broadening is Lorentzian which is not entirely accurate [1] but is generally accepted, because the inferred errors are relatively small [21]. Under these assumptions we determine the Stark width from the Voigt profile using the relation, $W_{\mathrm{V}} \approx 0.5346W_{\mathrm{L}} + \sqrt{0.2166W_{\mathrm{L}}^2 + W_{\mathrm{G}}^2}$ developed by Olivero and Longbothum [22], where W_{V}, W_{L}, W_{G} stand for the widths of the Voigt, Lorentzian ($W_{\mathrm{L}} = W_{\mathrm{VdW}} + W_{\mathrm{Stark}}$) and Gaussian ($W_{\mathrm{G}} = \sqrt{W_{\mathrm{instr}}^2 + W_{\mathrm{Dopp}}^2}$) profiles, respectively. The Stark width is the sole unknown here and can be varied to obtain the best fit between the experimental spectral line and the calculated Voigt profile. Figure 6 shows the raw H_α profiles recorded at two different times and the best Voigt fits with the corresponding calculated Stark FWHM and FWHA values. The experimental and the calculated profiles compare very well, even in the case of high SNR, such as the in the beginning of the discharge at $t = 2.581$ μs (see figure 6(a)).

Table 1. Instrumental, VdW and Doppler broadening widths.

T_g (K)	Instr. (Å)	VdW (Å)	Doppler (Å)
750	0.32	0.557	0.129
900	0.32	0.491	0.141

The evolution of plasma density as inferred from the H_α FWHA as a function of time is shown in figure 7, together with intensity of H_α emission, intensity of the broadband emission at HAL = 8 mm and the driving pulse envelope (indicating the 'RF ON' part of the duty cycle). The emission of H_α emerges with the ignition of the channel ($t \approx 1.4$ μs) before it reaches the liquid. The density peaks after plasma reaches the liquid ($t \approx 3$ μs), followed by gradual decline and eventual plateau for the remainder of the 'RF ON' phase. When the RF switched off at $t = 10$ μs, a substantial increase in emission and density is observed. This is a reignition phase, which has been observed in free-space APPJs [23–25] and in jets interacting with targets [9, 17]. The reignition occurs because the dielectric tube

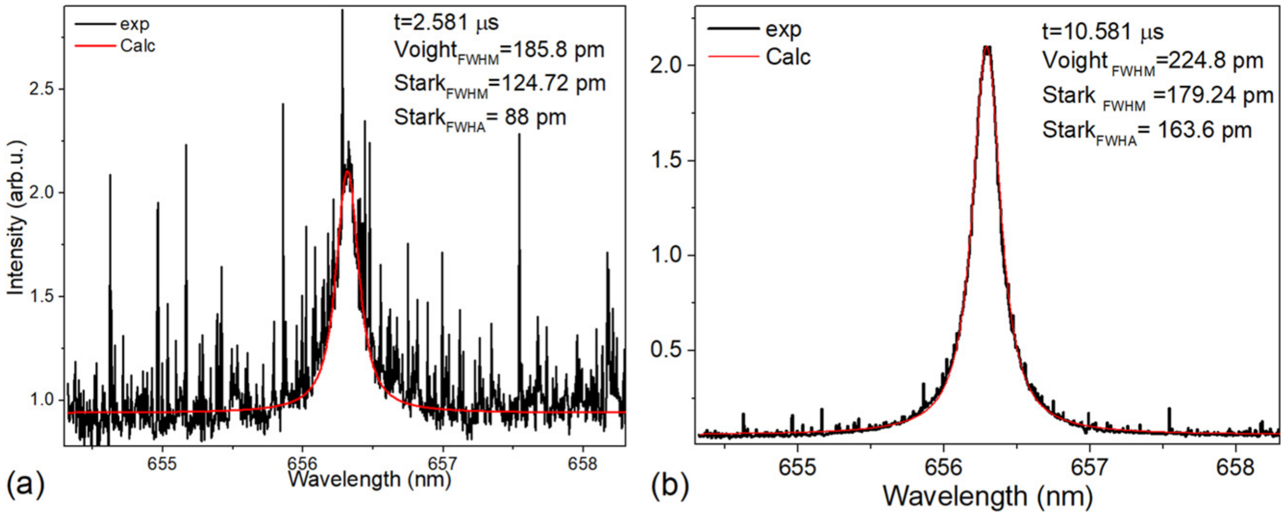

Figure 6. H_α profile: experimental versus calculated Voigt (a) at $t = 2.581\ \mu$s (b) at $t = 10.581\ \mu$s.

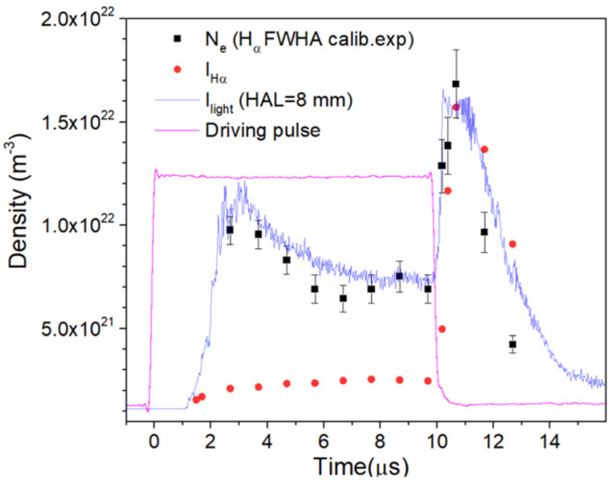

Figure 7. Temporal evolution of N_e, broadband light intensity at HAL = 8 mm (I_{light}) and the intensity of H_α emission ($I_{H\alpha}$).

around the central electrode in the jet is charged during the 'RF ON' phase and is discharged with the onset of the 'RF OFF' phase. The electron density reaches a maximum just above 1.7×10^{22} m^{-3} roughly 0.5 μs after RF is switched off. Both emission of H_α and broadband light also peak at the same time, but it is worth noting that the peak intensity of H_α during the reignition phase is an order of magnitude higher when compared to the peak value observed during the 'RF ON' phase. This is likely due to rapid introduction of hydrogen, dissociated from the water. Rapid evaporation of the liquid and dissociation of the water molecules would require a sharp current spike, owing to the discharge from the dielectric tube surrounding the electrode.

3.4. Thomson scattering

The analysis of the TS signals was detailed in the recent work by Oldham *et al* [26] and here we follow exactly the same methodology using the same tools. Nonetheless, a short description of the methods follows below to recap the approach. TS occurs in two distinctive regimes [27]: coherent and incoherent. The incoherent regime implies that the laser interacts with individual electrons in the Debye sphere and the scattered photons are therefore not phase correlated. In this case the spectral dispersion profile has a Gaussian shape, owning to the Maxwellian electron velocity distribution. The electron temperature is then readily obtained from the FWHM of the TS profile. The electron density is related to the intensity of the TS signal and to determine its absolute value one needs a calibration by either Rayleigh or Raman scattering from a gas with known scattering cross-section and at known concentration. This method is referred to as 'intensity calibration' and further details can be found in the work of van Gessel *et al* [19] The TS is frequently incoherent in laboratory plasmas with low density ($\leqslant 10^{21}$ m^{-3}).

Coherent TS occurs at higher N_e/T_e ratios, when the laser field incites waves in the plasma, so the electrons (and ions) interact with the laser field collectively, i.e. the laser is scattered by electronic and ionic acoustic waves. In atmospheric pressure plasmas the ionic component is very narrow, owing to low temperature of the heavy particles and is centered around the laser wavelength, similarly with the Rayleigh scattering from the neutral particles. Consequently, it is filtered out together with Rayleigh component (using the BNF in our system). The scattering on the electron wave can still be seen when the filter bandwidth is narrow enough, and they create a unique profile shape, defined by a scattering parameter $\alpha = \frac{\lambda_l}{4\pi\ \sin(\theta/2)\lambda_D}$, with λ_l being the laser wavelength, scattering angle θ and Debye length λ_D. The Debye length is essentially a length scale on which the electrons are shielded from external electric fields and is defined via $\lambda_D = \sqrt{\frac{\varepsilon_0 k_B T_e}{q_e^2 n_e}}$, where ε_0 is the permittivity of free space and q_e is the elementary charge. Therefore, the limit $\alpha \ll 1$ implies that $\lambda_l \ll \lambda_D$, the scattering occurs within Debye sphere, hence the electrons scatter the photons individually and the resulting photon distribution will be Gaussian due to the Doppler effect. When

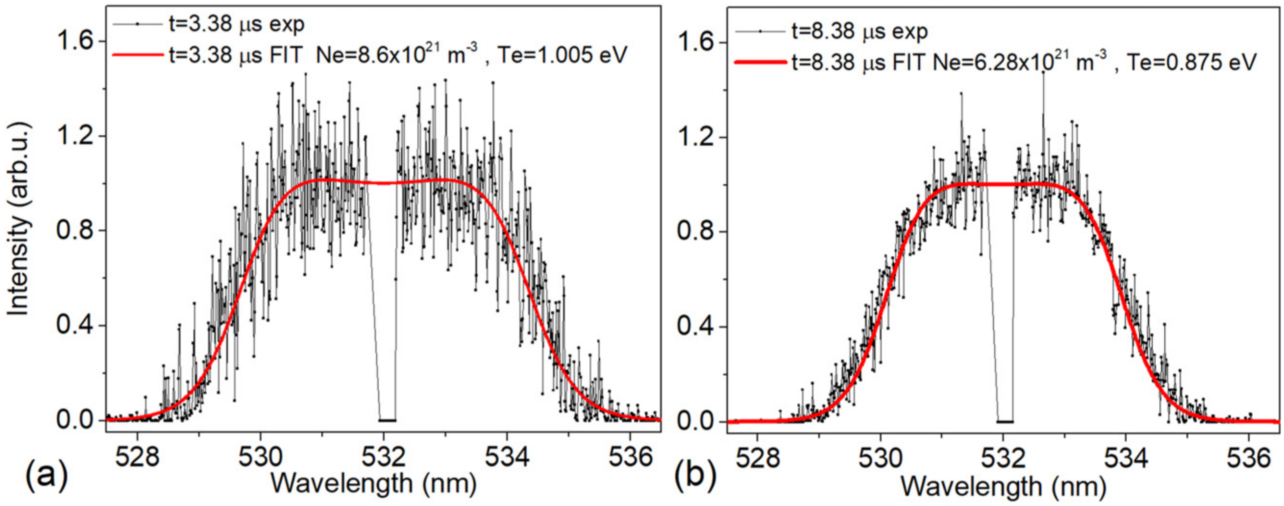

Figure 8. Measured TS signals and best fitting calculated spectrums at two different times.

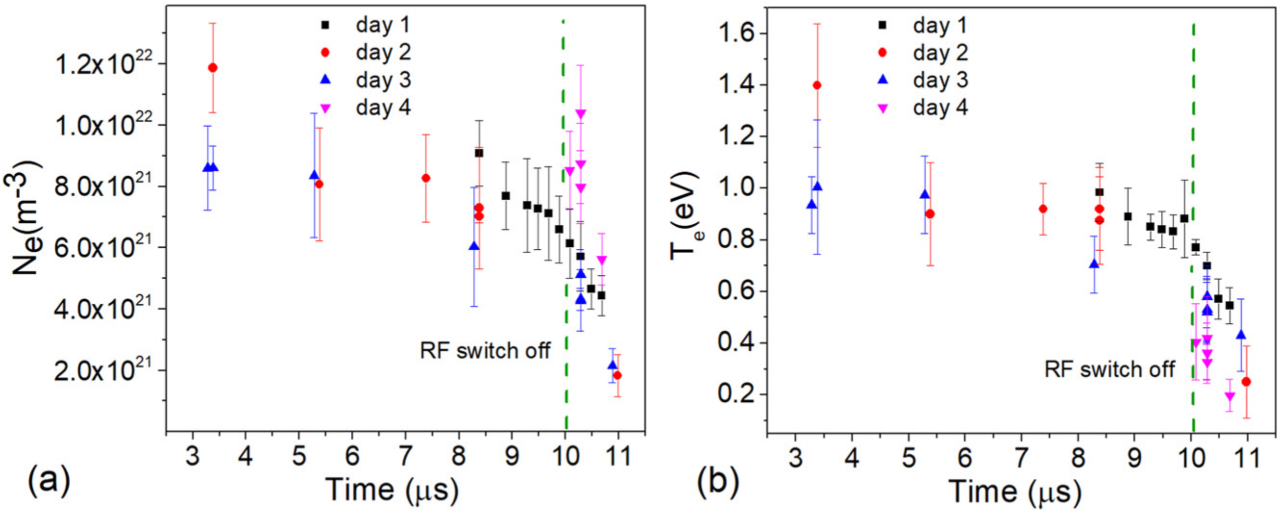

Figure 9. (a) Temporal evolution of N_e measured with TS (b) Temporal evolution of T_e measured with TS.

$\alpha \geqslant 0.2$ the $\lambda_l \gg \lambda_D$, so the laser wave does not 'see' individual electrons and the scattering is collective/coherent character. The shape of the Thomson profile in this case no longer Gaussian and has a specific shape, strongly influenced by the value of α, to the point that the value of α can be uniquely determined from the shape of TS signal. This case is called 'shape calibration' and it is very convenient because it allows determination of N_e and T_e without additional scattering (Rayleigh or Raman), as in the case of incoherent scattering. One can still use intensity calibration for coherent TS, in fact the combination of the two can have some advantages as was shown by van der Mullen *et al* [28].

The Thomson signals collected in this work are dominantly non-Gaussian, indicating coherent scattering regime. The processing of the signal to determine the plasma parameters requires either shape-fitting or intensity fitting with correction for transient effects, as outlined in the work of Obrusník *et al* [29]. Shape-calibration procedure was described in the work of Huang and Hieftje [30] which also details the analytical calculation of the TS spectrum. The procedure relies on the recognition that the spectrum shape is uniquely defined by the value of α. Therefore, to find the best fit to an experimental spectrum one must assume values for N_e and T_e, calculate the corresponding α and compute the full Thomson spectrum, which is then compared to the experimental. Details on the calculation procedure can be found in reference [26]. In the same work by Oldham *et al*, we have also used intensity calibration approach to cross-validate the two calibration techniques, showing a satisfactory convergence to similar values.

It must be noted that several works dealing with TS of APPJs have noticed a non-negligible Raman scattering contribution to the measured spectrum due to entrainment of ambient air into the plasma channel [7, 9, 25]. The TS spectra collected in this work exhibit no such contribution and nor do the spectra collected just before the ignition of the plasma. We have collected signals at $t \leqslant 1$ μs to check for Raman peaks

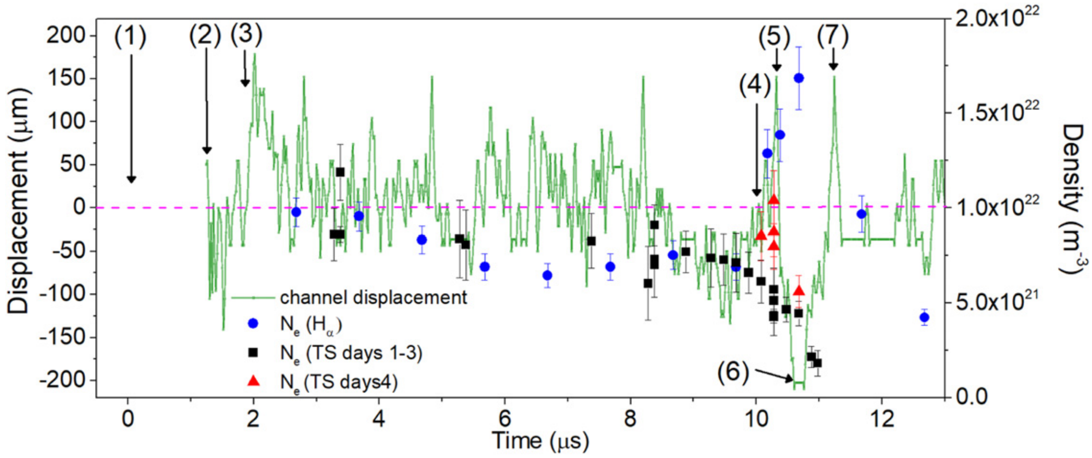

Figure 10. Electron density temporal evolution measured by Stark width of H_α and TS versus dislocation of the plasma channel. The dashed magenta line indicates the 0 μm dislocation, which is the average position where the channel is located throughout the cycle. Numbers and arrows indicate the following events: (1) RF is switched on (2) onset of plasma emission (3) plasma channel reaches the liquid (4) RF is switched off (5)–(7) major dislocation of the channel after the RF switch-off.

from scattering on N_2 and O_2, but no such peaks were found (figure 8).

The temporal evolution of N_e and T_e as measured by TS is shown in figure 9. The TS signals were collected across few days, spanning the time delays $2 \leqslant t \leqslant 11.5$ μs. The time-scan was done with some overlap in time delays, to test the repeatability of the measurements, given the intrinsic instability of plasmas in contact with liquids. The results shown in figure 9 are broken down by days.

4. Discussion of the results

The measurements made on different days were largely repeatable and yielded similar plasma parameters with overlapping error bars. However, the TS measurements made on days 1–3 did not appear to capture the reignition of the plasma channel after the termination of the 'RF ON' phase. Day 4 (see figure 9) was therefore dedicated to attempts of capturing the reignition with only a partial success.

The reason for this caveat was apparent when the densities measured by both approaches (Stark vs TS) were compared together with the dislocation of the plasma channel at HAL $=$ 8 mm, as shown in figure 10. At the presented plot the displacement of the channel is the spatial location of the peak of the emission of the plasma channel at HAL $= 8 \pm 0.25$ mm (averaged across 0.5 mm in the vertical direction) relatively to the averaged location throughout the whole 'RF ON' period. The data in figure 10 shows that both approaches captured similar densities until $t = 10$ μs. When the RF pulse was switched off—the TS measured density (days 1–3) plummets as the 'Stark' density climbs up and peaks. This disagreement coincides with the timing of the 'rapid swings' observed in the spatial position of the channel that occur after the 'switch-off' ($10 \leqslant t \leqslant 11.3$ μs). With respect to the average position during the 'RF on' cycle, the channel moves first approximately $+170$ μm one way and then swings to -200 μm and then again $+170$ μm. It is obvious that during these swings the laser–plasma overlap is lost or minimal, resulting in sharp decrease of the scattering signal. Two clarifications must be made: (1) the observed dislocation is the projection on the plane parallel to the plane in which the laser beam propagates (see setup sketch at figure 2) and (2) the measurement of the channel dislocation is a separate experiment; it does not happen simultaneously with any of the other measurements. However, we believe it represents qualitative behavior, while the amplitude and the actual direction of the dislocation in each RF cycle may vary.

The physical reason for these swings is likely the detachment of the channel from the liquid surface, which occurs right after the 'switch-off', see figures 4(m)–(p). As the channel moves to distances comparable with the laser beam radius—the cross-section between the plasma and the laser is diminished, causing low SNR in the measured TS spectrum. Also the center of the plasma channel is no longer probed by the laser, hence the measured electrons are less dense and colder. It is interesting to note that another major dislocation of the channel occurs at $2 \leqslant t \leqslant 3$ μs, with the peak approximately at 2.1 μs, which is when the plasma channels reaches the liquid surface. There is also a significant, non-stochastic deviation from oscillations around 0 μm at $8 \leqslant t \leqslant 10$ μs. While the physical cause for that is not clear, but since the amplitude of the deviation $\sim$100 μm the laser beam still overlaps sufficiently with the plasma channel and the measured electron density shows no significant decrease. This exemplifies the importance of the larger laser focal spot for measurements in unstable/oscillating filamentary plasmas.

We must note that every data point captured by TS was preceded by the alignment along two axes, as explained in section 2.2 and shown in figure 2, including measurements made between $10 \leqslant t \leqslant 11.3$ μs. This means that after the 'switch off' the channel location is stable enough to allow alignment, but not on the span of the long TS measurement (17 min). The measurements in days 1–3 were performed by one person, meaning that the alignment process was longer. Day 4 measurements were an attempt to capture the reignition with TS. Two person team was engaged, in order to streamline the alignment procedure with one person operating the micrometers that move the jet and the other person performing the data acquisition and simultaneous signal processing to determine the optimal positions. This allowed for faster laser alignment and transition to measurements earlier, although we did not time these transitions. The results did show an increase in the N_e values measured immediately after the RF 'switch off' phase but did not produce the sharp peak observed via light emission and Stark broadening analysis. The measured values were higher than the ones measured for $10 \leqslant t \leqslant 10.5$ μs on days 1–3 (see figure 9(a)), but at later times corresponding to the peak density of emission and line broadening ($t \approx 10.7$ μs) the TS measured density still plummets. One can notice that the this time also corresponds to the maximum dislocation of the channel, hence the laser beam–plasma overlap is lowest. Thus the attempt to capture the re-ignition in the plasma–liquid system was largely unsuccessful. The alignment of the system works well in the 'RF ON' time segment but fails after the RF 'switch-off'. On one hand, this demonstrates that behavior of the channel is unpredictable, once that the external electric field is removed. On the other hand, the measurements on day 4 show some success in measuring the re-ignition, with some correlation to faster transition from alignment to measurements.

It must be said that the reignition of the channel after the voltage switch-off was observed by means of TS before in the work by Hübner *et al* [25], while studying a 3.5 kV, 5 kHz Ar jet, in free space. APPJ in free space tend to be less filamentary and more spatially stable, hence it is likely that spatial oscillations did not incur a problem for TS in that work, therefore the specific system is the likely culprit for the shortfalls of TS application in our experiment.

5. Summary and conclusions

This work describes detailed characterization of the RF jet operating in contact with liquid. The formed plasma is filamentary and not entirely stable in space. The formation of the channel was studied with fast gated imaging, showing that plasma first appears on the edge of the electrode at $t \approx 1.3$ μs, with respect to the switching the 'RF on'. The plasma channel reaches the liquid surface at $t \approx 2.1$ μs. After 10 μs the RF is switched off and the plasma immediately recedes from the liquid, towards the middle of the gap. At the same time the intensity of the emission in the rest of the channel (HAL = 6–10 mm) intensifies due to the reignition of the channel, with peak intensity at $t \approx 11$ μs. The reignition 'candle' is over at $t \approx 14$ μs and the emission then recedes from the electrode, towards the center of the gap. By the time $t = 20$ μs the emission is mostly gone.

Gas temperature was also measured in this work by means of Rayleigh scattering. Gas temperature stays in the range $750 \leqslant T_g \leqslant 850$ K during the 'RF ON' phase and slightly increases in the reignition phase, subsequently going back to approximately 750 K. The gas temperature values were used for informed estimation of the Doppler and VdW broadening of hydrogen Balmer α line.

The Stark width (FWHA) of this line was used to measure the electron density evolution in the time segment $2 \leqslant t \leqslant 12$ μs. The H_α line emission was detected right after the plasma ignition, but it only became broad enough to analyze at $t = 2.7$ μs. At that point the density was determined to be approximately 9×10^{21} m^{-3}, decreasing gradually to 6×10^{21} m^{-3} and plateauing until the RF switches off. The reignition of the channel is emphasized in quick 'boost' of the electron density to the peak value of 1.7×10^{22} m^{-3}, obtained at $t \approx 10.6$ μs.

TS was used to measures N_e and T_e. Electron temperature is mostly constant during the 'RF ON' stage, at $T_e = 0.9 \pm 0.1$ eV. During the 'RF ON' phase the density from TS agrees with that determined by Stark broadening. However, TS fails to capture the reignition stage and the measured density decreases right after RF switches off.

Inspection of the oscillation and dislocation of the plasma channel reveals the apparent reason for TS failing to capture the reignition stage. The plasma filament does oscillate spatially for $3 \leqslant t \leqslant 10$ μs, in a stochastic fashion. At that time segment the oscillation amplitude is mostly below ± 100 μm. Consequently, the large diameter of the laser beam (318 μm) ensures that laser overlaps with the filament and despite oscillations the laser photons are scattered. For $t > 10$ μs, the channel exhibits large, non-stochastic movements, before the channel reaches the liquid and after the RF switches off. These dislocations have an amplitude greater than 150 μm, and the direction switches rapidly three times within 1.5 μs. Large swings in the position of the channel suggest that the laser does not probe the very core of the plasma, but rather the much less dense surroundings. Alignment of the plasma to the laser and to the monochromator slit does not resolve this issue, as the swings appear to change direction on a timescale that is longer than the alignment process, but shorter than the signal collection in this work. Hence, during the pre-measurement alignment the channel is localized but is later 'lost' during the measurement itself.

Plasma parameters are needed for correct modeling of plasma-induced chemistry [18]. They are also necessary for understanding the plasma–liquid interaction and the impact of the plasma on the liquid. The measurements described in this manuscript were employed in the follow-up work, described in reference [26], where the potential of a floating surface in contact with the plasma is calculated using the measured plasma density and temperature. The correlation of the floating potential to the reduction potential near plasma–liquid interface is further conducted and the corresponding modeling framework is described. The above work also shows how the plasma parameters (density and temperature) and the corresponding floating potential scale with the RF power for range of 20–50 W. Since Ar RF jets are quite popular in low-temperature plasma community we expect that this data will be found useful, because so far plasma of RF jets in contact with liquid were not studied in detail, at least to the best of our knowledge. The body of work where plasma jet in contact with liquid was characterized was briefly reviewed in the introduction. It is evident that the main difference in plasma parameters obtained with different power supplies is in the electron temperature: several works used kHz excitation for Ar and He jets and obtained T_e values of 2–4 eV, while in our study of Ar jet with RF excitation the temperature does not exceed 1 eV. The plasma densities are similar between our RF source and kHz sources.

In addition to the full characterization of the plasma in this system, this work constitutes a cautionary tale for the application of TS to characterizing plasma jets in contact with liquids. With filamentary plasmas it is of utmost importance to monitor and correlate laser-based diagnostics (such as TS) to the spatial behavior of the plasma channel. Failure to do so might result in missing out on physical phenomena, or erroneous measurement of plasma parameters. Nevertheless, we are of the opinion that such systems, where plasmas are filamentary and not spatially stable, are attractive for certain applications, therefore they will continue to be used and studied despite the plasma diagnostic challenges. TS will likely continue being used by the atmospheric plasma community as it constitutes a direct T_e measurement, and furthermore, allows measurement of N_e when its value is not high enough to use spectral line methods. Therefore, the identification of the TS shortcomings is necessary as are approaches to mediate them.

Acknowledgments

The work by Shurik Yatom is supported by the Princeton Collaborative Research Facility (PCRF), which is supported by the US Department of Energy (DOE) under Contract No. DE-AC02-09CH11466. Plasma diagnostic resources used in this work were provided by the PCRF. Trey Oldham and Elijah Thimsen acknowledge financial support from the US Department of Energy under Award No. DE-SC0020352.

Data availability statement

The data that support the findings of this study are available upon reasonable request from the authors.

ORCID iDs

Shurik Yatom https://orcid.org/0000-0001-8716-8487
Trey Oldham https://orcid.org/0000-0002-4058-1490
Elijah Thimsen https://orcid.org/0000-0002-7619-0926

References

[1] Gigosos M A, González M Á and Cardeñoso V 2003 *Spectrochim. Acta* B **58** 1489–504
[2] Kunze H-J 2009 *Introduction to Plasma Spectroscopy* (Berlin: Springer)
[3] Griem H R 1997 *Principles of Plasma Spectroscopy* (Cambridge: Cambridge University Press)
[4] Yatom S and Raitses Y 2020 *Phys. Chem. Chem. Phys.* **22** 20837–50
[5] Muraoka K and Kono A 2011 *J. Phys. D: Appl. Phys.* **44** 043001
[6] Hübner S, Sousa J S, van der Mullen J and Graham W G 2017 *Plasma Sources Sci. Technol.* **24** 054005
[7] van Gessel B, Brandenburg R and Bruggeman P 2013 *Appl. Phys. Lett.* **103** 064103
[8] Simeni M S, Roettgen A, Petrishchev V, Frederickson K and Adamovich I V 2016 *Plasma Sources Sci. Technol.* **25** 064005
[9] Klarenaar B L M, Guaitella O, Engeln R and Sobota A 2018 *Plasma Sources Sci. Technol.* **27** 085004
[10] Palomares J M, Hübner S, Carbone E A D, de Vries N, van Veldhuizen E M, Sola A, Gamero A and van der Mullen J J A M 2012 *Spectrochim. Acta* B **73** 39–47
[11] Slikboer E and Walsh J 2021 *Sci. Rep.* **11** 17749
[12] Slikboer E and Walsh J L 2021 *J. Phys. D: Appl. Phys.* **54** 325201
[13] Yatom S and Krasik Y E 2014 *J. Phys. D: Appl. Phys.* **47** 215202
[14] Oldham T, Chen M, Sharkey S, Parker K M and Thimsen E 2020 *J. Phys. D: Appl. Phys.* **53** 165202
[15] Klarenaar B L M, Brehmer F, Welzel S, van der Meiden H J, van de Sanden M C M and Engeln R 2015 *Rev. Sci. Instrum.* **86** 046106
[16] Carbone E A D, Palomares J M, Hübner S, Iordanova E and van der Mullen J J A M 2012 *J. Inst.* **7** C01016
[17] Yatom S, Luo Y, Xiong Q and Bruggeman P J 2017 *J. Phys. D: Appl. Phys.* **50** 415204
[18] Luo Y, Lietz A M, Yatom S, Kushner M J and Bruggeman P J 2019 *J. Phys. D: Appl. Phys.* **52** 044003
[19] van Gessel A F H, Carbone E A D, Bruggeman P J and van der Mullen J J A M 2012 *Plasma Sources Sci. Technol.* **21** 015003
[20] Yubero C, Calzada M D and Garcia M C 2005 *J. Phys. Soc. Japan* **74** 2249–54
[21] Konjević N, Ivković M and Sakan N 2012 *Spectrochim. Acta* B **76** 16–26
[22] Olivero J J and Longbothum R L 1977 *J. Quant. Spectrosc. Radiat. Transfer* **17** 233–6
[23] Kim S J, Chung T H and Bae S H 2010 *Phys. Plasmas* **17** 053504
[24] Karakas E and Laroussi M 2010 *J. Appl. Phys.* **108** 063305
[25] Hübner S, Hofmann S, van Veldhuizen E M and Bruggeman P J 2013 *Plasma Sources Sci. Technol.* **22** 065011
[26] Oldham T, Yatom S and Thimsen E 2022 Plasma parameters and the reduction potential at a plasma-liquid interface *Phys. Chem.* (submitted)
[27] Hutchinson I H 2002 *Principles of Plasma Diagnostics* (Cambridge: Cambridge University Press)
[28] van der Mullen J, Atanasova M, Obrusník A and Zajíčková L 2020 *J. Anal. At. Spectrom.* **35** 2064–74
[29] Obrusník A, Synek P, Hübner S, van der Mullen J J A M, Zajíčková L and Nijdam S 2016 *Plasma Sources Sci. Technol.* **25** 055018
[30] Huang M and Hieftje G M 1989 *Spectrochim. Acta* B **44** 291–305